Joint Air-Fuel Ratio and Torque Regulation using Secondary Cylinder Air Flow Actuators[1]

A. G. Stefanopoulou[2], J. A. Cook[3], J. W. Grizzle[4], J. S. Freudenberg[4]

Abstract

Actuation schemes exist that permit the joint management of air and fuel flow into the cylinders of a spark ignition engine. With the exception of drive by wire systems, to-date, the transient control aspects of these schemes, collectively refered to here as *secondary cylinder air flow actuators*, has not received any attention from the control community. This paper takes a first step in the analysis of the simultaneous dynamic control of air fuel ratio and torque response using secondary actuators placed before the intake ports of the cylinders, when used in combination with standard fuel injectors and primary throttle regulated by the driver. The emphasis is on basic issues of designing a feedforward scheme to enhance actuator authority for feedback control, and the fundamental multi-variable nature of the feedback problem. Enhanced transient air-to-fuel ratio performance improvement is shown to be possible without sacrificing engine torque response with respect to a conventional engine. In addition, this is achieved with overall higher manifold pressure, offering the *possibility* of reduced pumping losses in the engine, depending on the actual actuation scheme employed.

1 Introduction.

Environmental regulations continue to drive research on improved vehicle emissions and fuel economy. Achieving cleaner burning and more fuel-efficient automobiles without compromising drivability is a challenging task. The engine management system has to satisfy rapid driver commands for acceleration. In conventional engines, the driver controls the amount of air inside the intake manifold through a mechanical linkage between the pedal and throttle mechanism. Rapid changes in the throttle position strongly influence the cylinder air charging process, mixture formation and transient performance of the engine (Manz, 1992). The changes in the air charge appear topologically as output disturbances in the air-to-fuel ratio (A/F) control loop, and ultimately affect the Three Way Catalyst (TWC) efficiency through A/F deviations from stoichiometry. The control of the A/F around stoichiometry is usually based on regulating the fuel flow to follow the air flow changes imposed by the driver. The associated feedback control system, however, does not have sufficient bandwidth to reject these disturbances due to the long "transport" delay in the induction-compression-combustion-exhaust cycle. Current A/F control practice relies heavily on feedforward cancelation of the estimated air charge disturbance, which makes it vulnerable to model uncertainties. For this reason, there has been a considerable research effort in developing alternative sensing and actuating techniques that can improve A/F control.

Various studies on A/F control can be roughly divided into two categories. The work represented by (Moraal, 1995; Hendricks et al., 1993) and references therein address the scarcity and nonlinearity of the conventional sensor set. The emphasis in these studies is on the reconstruction of signals available for feedback, and the accurate and robust knowledge of the system states. The second category of studies addresses new engine configurations, namely, the introduction of new actuators that regulate the air flow into the manifold depending on the primary throttle (driver's pedal) movement. Developments in the area of drive-by-wire (DBW) throttle systems (Emtage et al., 1991) and electronic throttle control (ETC) (Chang et al., 1993; Bidan et al., 1993) revive early investigations of combining air control in addition to fuel control (Prabhakar et al., 1975) to improve A/F control and reduce engine emissions. Obviously, the additional actuators do not alleviate the feedback limitation in the fuel loop, but provide an additional degree of freedom to better manage the tradeoff between fast torque response and tight A/F. Although promising results have been shown in (Chang et al., 1993; Bidan et al., 1993) and references therein, the DBW system decouples the engine from the driver and requires additional fail-safe mechanisms.

In view of these difficulties and in light of newly developed mechanisms that allow cylinder air flow control for reduction of pumping losses (load control), we

[2] Mechanical and Environmental Engineering Department, University of California, Santa Barbara, CA 93106-5070

[3] Ford Motor Company, Scientific Research Laboratory, PO Box 2053, Mail Drop 2036 SRL, Dearborn, MI 48121

[4] Control Systems Laboratory, Department of Electrical Engineering and Computer Science, University of Michigan, Ann Arbor, MI 48109-2122

investigate the potential ability of these secondary actuators to improve A/F control and, thus, contribute in emission reduction. The best cylinder flow control functionality is achieved by a camless engine (Schecter and Levin, 1996). Other studies (Tuttle, 1980; Ma, 1988) have shown that intake valve closing can be used to control engine torque and reduce pumping losses; the latter is achieved by reducing the need to throttle the air flow through the primary throttle body. In (Gray, 1988), supplementary valves in the inlet port or manifolds are discussed as an alternative solution to fully variable valve timing. In a recent experimental work (Vogel et al., 1996), the authors compare the pumping work of an engine equipped with secondary valves with the theoretical pumping work of an ideal, early-closing intake valve system.

The goal of this paper is to investigate if secondary actuators in the inlet port of the cylinders (Fig. 1) can be used in coordination with the fuel injectors to achieve (i) tight A/F control, (ii) good tracking of torque demand while maintaining conditions for low pumping losses. We are going to investigate the feasibility of the secondary actuators concept based on some paper studies and simulations, without actual hardware for experimental validation. Hence we use a simplistic model for the secondary actuators; details will depend on the eventual hardware implementation. Our work is intended in part to identify whether any fundamental difficulties exist with the secondary actuators concept that would preclude further development. We also wish to compare, to the extent possible, the potential performance of the secondary actuators with respect to other schemes. In fact, although our work identified issues that must be addressed in the use of secondary cylinder air flow actuators (i.e., the actuator authority in different operating ranges), the concept shows sufficient promise to merit further development. Indeed additional work on secondary actuators is ongoing (Kang and Grizzle, 1998; Kang and Grizzle, 1999).

For the control analysis and design, the engine model is based on the initial work in (Crossley and Cook, 1991) and (Foss et al., 1989). The engine model developed in (Crossley and Cook, 1991) has been modified to describe the effects of secondary actuators placed before the intake ports of the cylinders. The secondary actuators are modeled as a gain (θ_c) multiplying the conventional mass air flow into the cylinders. In the new control scheme, the primary throttle is still regulated by the driver, alleviating safety related problems. It is assumed that a reliable and accurate torque measurement is available, such as could be obtained from an in-cylinder pressure sensor (Powell, 1993) or accurate crankangle acceleration measurements (Srinivasan et al., 1992). A linear EGO sensor for A/F measurement is also supposed.

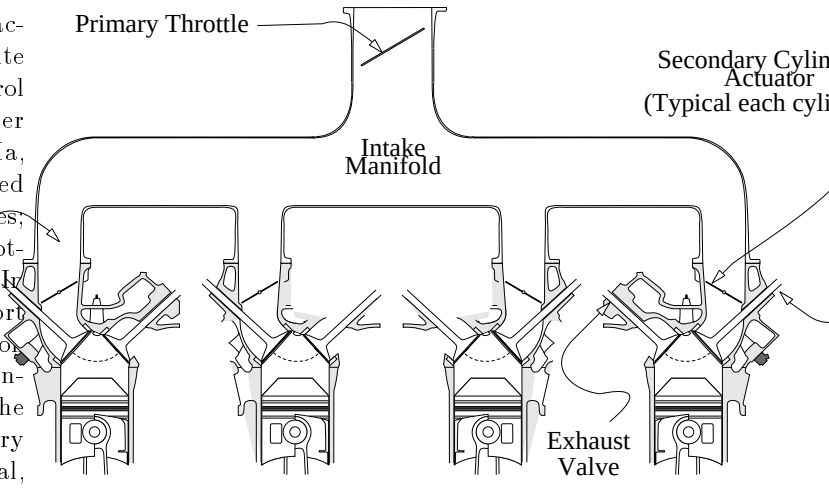

Figure 1: Schematic representation of 4-cylinder engine with secondary cylinder air flow actuators.

The contributions of the analysis done here is the identification of the different control authority regions for regulating the steady-state air flow into the cylinders. This result, although well known in the thermodynamic community ((Heywood, 1988), pg. 307), has not been previously addressed by control engineers.

The paper is organized as follows. Definitions of the variables and their units are provided in the next section. An overview of the model is given in Section 3. Section 4 discusses the dynamics of the nonlinear breathing process after the introduction of the secondary actuators; the nonlinear feedforward design of the set points for the secondary actuators is discussed in Section 5. The relationship between the primary throttle position and the torque set-point for the control scheme is described in Section 6. The linear feedback design is discussed in Section 7. Results and comparisons are given in Section 8. Conclusions and future work are discussed in Section 9.

2 Nomenclature.

A/F	air-fuel ratio
$\dot{m}$	mass flow, g/sec
N	flywheel speed, rad/sec
P	pressure, bar
T_q	shaft torque, Nm
T_b	engine brake torque, Nm
θ	primary throttle angle, degrees
θ_c	gain due to secondary actuators, uniteless $(0 \div 1)$

3 Engine Model.

This section gives an overview of the nonlinear mathematical representation of the engine model developed in (Crossley and Cook, 1991) and (Foss et al., 1989), and the modification used to describe the use of secondary actuators. The model is a continuous-time nonlinear, low-frequency[1] phenomenological model with uniform pulse homogeneous charge, and lumped parameter approximation of breathing and rotational dynamics. The nonlinear mathematical representation of the engine model with secondary actuators is constructed, based on physical engine characteristics, by modulating the mass air flow into the cylinders by a simple multiplication with a signal (θ_c). The signal (θ_c) takes values from 0 (high modulation) to 1 (no modulation). Figure 2 shows the block diagram of the engine model with secondary actuators.

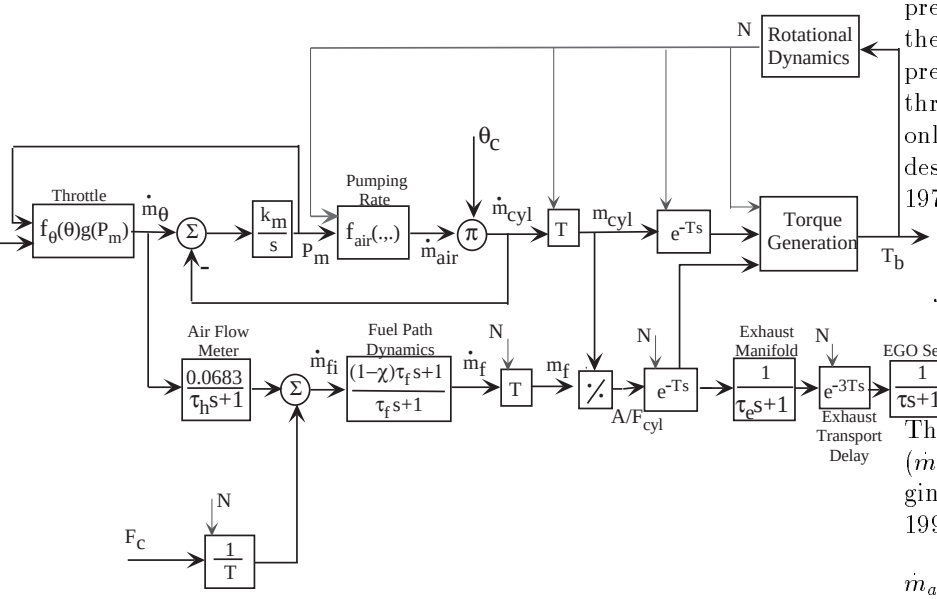

Figure 2: Engine model with secondary actuators.

Breathing process dynamics

The manifold was analyzed as a single control volume with the throttle plate controlling mass air flow into the manifold, and the engine cylinders in combination with the secondary actuators controlling mass air flow out of the manifold. Based on the "Filling and Emptying Models" described in (Heywood, 1988), the manifold acts as a plenum, where the rate of change of the manifold pressure (P_m) is proportional to the mass air flow rate into the manifold ($\dot{m}_\theta$) minus the pumping mass air flow rate ($\dot{m}_{cyl}$) into the cylinders. The manifold dynamics are described by the following first order differential equation (see (Powell and Cook, 1987)) that relates the rate of change of the manifold pressure (P_m) to the flow rates into and out of the manifold ($\dot{m}_\theta$ and $\dot{m}_{cyl}$, respectively)

$$\frac{d}{dt}P_m = K_m(\dot{m}_\theta - \dot{m}_{cyl}), \text{ where } K_m = \frac{R \cdot T_m}{V_m} . \quad (1)$$

Based on the nominal manifold temperature (T_m), the manifold volume (V_m), and the specific gas constant $R = 287$ J/kgK, the constant K_m was calculated to be equal to 0.413 bar/g. This model is an engine event averaged representation of the intake manifold filling dynamics. The dynamic manifold pressure obtained by this model is not the instantaneous manifold pressure. The mass air flow rate into the manifold ($\dot{m}_\theta$) through the primary throttle body is a function of throttle angle (θ), the upstream pressure (P_o), which we assume to be the atmospheric, i.e., $P_o = 1$ bar, and the downstream pressure, which is the manifold pressure (P_m). When the manifold pressure is less than half of atmospheric pressure, i.e., $P_m/P_o < 0.5$, the flow $\dot{m}_\theta$ through the throttle body is described as sonic flow and depends only on the primary throttle position. The function describing $\dot{m}_\theta$ in the two flow regimes is given in (Novak, 1977) and (Prabakhar, 1975) by :

$$\dot{m}_\theta = f_\theta(\theta)g(P_m)$$
$$f_\theta(\theta) = 2.821 - 0.05231\theta + 0.10299\theta^2 - 0.00063\theta^3$$
$$g(P_m) = \begin{cases} 1 & \text{if } P_m \le P_o/2 \\ \frac{2}{P_O}\sqrt{P_m P_o - P_m^2} & \text{if } P_m > P_o/2. \end{cases} \quad (2)$$

The conventional engine pumping mass air flow rate ($\dot{m}_{air}$) is a function of manifold pressure (P_m) and engine speed (N) and is given in (Crossley and Cook, 1991) by :

$$\dot{m}_{air} = f_{air}(N, P_m) = -0.366 + 0.08979NP_m - 0.0337NP_m^2 + 0$$

The secondary actuators modulate the air flow rate out of the manifold and into the cylinders, so the mass air flow rate into the cylinders ($\dot{m}_{cyl}$) is modeled by :

$$\dot{m}_{cyl} = \theta_c \cdot \dot{m}_{air}, \quad (4)$$

where, θ_c is indirectly related to the geometric characteristics of an actuator that realizes secondary cylinder flow control in the intake port of the cylinder. This model is intended to capture the average flow rate of air into the cylinder over an intake event, and not the instantaneous, crank-angle by crank-angle, flow rate. The mass air flow into the cylinders is in general expressible as $\dot{m}_{cyl}(t) = f_{cyl}(p_r(t), N(t), v(t))$, where $p_r(t)$ is the pressure ratio at the intake valve, and $v(t)$ is the physical actuator signal. Such an instantaneous (or

[1] In this model mass flow rate, manifold pressure, and torque are represented by their average values over an engine event.

crank-angle) dependent model would be unwieldy for control design, and hence, we assume that a mean-value approximation of the cylinder air flow modulation can be identified via experimental data or via averaging the response obtained by simulations of a crank-angle based model (Ashhab et al., 1998; Moraal et al., 1993; Moraal et al., 1995). The mean-value model can be defined with a nonlinear static map $\dot{m}_{cyl} = \underline{f}_{cyl}(P_m, N, v)$, or equivalently, with a nonlinear gain $\theta_c = \theta_c(P_m, N, v)$ that modulates the nominal cylinder air flow, $\dot{m}_{air}(P_m, N)$, based on the equation $\dot{m}_{cyl}(P_m, N, v) = \theta_c(P_m, N, v) \cdot \dot{m}_{air}(P_m, N)$. In this work, the nonlinear gain θ_c is defined as the control signal as shown in Eq. 4. This model allows us to capture the mean value effect of a wide variety of devices that allow modulation of cylinder air flow such as secondary poppet or rotational valves, shutters, and variable camshaft or valve timing.

Process delays

The discrete nature of the combustion process causes delays in the signal paths: between the mass charge formation and the torque generation there exists a delay equal to the compression stroke duration, (T), and between the exhaust manifold and the exhaust gas oxygen (EGO) sensor there exists a delay which equals 3 times the intake event duration, $(3T)$. The event T is calculated by $T = \frac{900}{\pi N}$ sec.

Exhaust process dynamics

The dynamics of the exhaust manifold and the linear EGO sensor are modeled by a first order differential equation with time constant $\tau_e = 0.15$ sec and $\tau = 0.20$ sec, respectively.

Fuel path dynamics

The fuel puddling dynamics are important in accurate transient A/F control ((Chang et al., 1993), (Hendricks et al., 1993), and (Nishiyama et al., 1989)). In general, it is difficult to accurately model the fuel puddling dynamics (Moraal, 1995) because the parameters of the model depend strongly on the fuel characteristics, air backflow, and the temperature of the engine during operation (Turin and Geering, 1995). The model for the fuel puddling dynamics for a conventional injection/intake system is given in (Aquino, 1981) by

$$\begin{aligned} \tfrac{d}{dt}\dot{m}_{fp}(t) &= -\tfrac{1}{\tau_f}\dot{m}_{fp}(t) + \chi\dot{m}_{fi}(t) \\ \tfrac{d}{dt}\dot{m}_{f}(t) &= (1-\chi)\dot{m}_{fi}(t) + \tfrac{1}{\tau_f}\dot{m}_{fp}(t) \end{aligned}$$

where, $\dot{m}_{fi}$: injected fuel flow (Kg/sec) ,
$\dot{m}_{fp}$: fuel film mass flow (Kg/sec) ,
$\dot{m}_{f}$: cylinder port fuel mass flow (Kg/sec) ,
and χ : fraction of the injected fuel which is deposited on the manifold as fuel film.

We stress here that the secondary actuators affect the characteristics of backflow and temperature of the surface where the fuel is injected, and thus the uncertainty in the fuel path dynamics is an important consideration in the control design phase. The nominal values of χ and τ_f are chosen from (Aquino, 1981):

$\dot{m}_f = \frac{(1-X)\tau_f s+1}{\tau_f s+1}\dot{m}_{fi}, where$
$X = 0.3 + \frac{0.7}{90}\theta = 0.3 + \frac{0.7}{90}10 = 0.38,$
$\theta = 10$: angle in degrees of the primary throttle,
and $\tau_f = 0.1$ sec, resulting in

$$\dot{m}_f = \frac{0.062 \cdot s + 1}{0.1 \cdot s + 1}\dot{m}_{fi}. \tag{6}$$

Adequate transient A/F control during rapid changes in the throttle position by the driver requires feedforward compensation of the fuel command since the inherent delay in the A/F feedback loop prohibits rapid corrections through the feedback fuel command. The feedforward fuel command is regulated on the basis of the estimated cylinder air charge. The estimated cylinder air charge is calculated based on the mass air flow measurement at the mass air flow sensor (hot wire anemometer positioned upstream of the throttle body), and integrated during the intake event. The estimated cylinder air charge is divided by 14.64 (nominal A/F) to provide the feedforward fuel flow command used in the A/F loop. The dynamics of the air flow meter are modeled by a first order lag with a time constant $\tau_h = 0.13$ sec.

Torque generation

The torque generated by an engine depends on the ignition of the cylinder charge, the mixture formation, and engine specific physical parameters. Analytical curve fitting techniques are applied to dynamometer-engine experimental data in (Crossley and Cook, 1991) to estimate the steady-state brake torque generation given by:

$$\begin{aligned} T_b = \quad & -181.3 + 379.36 m_{cyl} + 21.91 A/F - 0.85 A/F^2 + 0.26 \\ & 0.027N - 0.000107N^2 + 0.00048N\sigma + 2.55\sigma m_{cyl} - 0. \end{aligned}$$

where,
m_{cyl} : mass air charge (g/intake event), $m_{cyl} = \dot{m}_{cyl}T = n$
A/F : air-to-fuel ratio ,
σ : degrees of spark advance before top dead center,
N : engine speed (rad/sec) , and
m_e : exhaust gas recirculation (g/intake event).

For simplicity in this study, the above equation was used with spark advance equal to 30 degrees ($\sigma = 30$), and exhaust gas recirculation equal to zero ($m_e = 0$).

(5)

Rotational dynamics

A very simplified model of the rotational dynamics is used for the engine with the secondary actuators model. The rotational motion of the engine crankshaft is given

in terms of the engine and the vehicle moment of inertia (J), angular acceleration ($\dot{N}$ in rad/sec^2), and the difference between the net torque generated by the engine (T_b in Nm) and the load torque on the shaft (T_l in Nm):

$$\Sigma T = T_b - T_l = (J\frac{2\pi}{60})\dot{N}. \tag{8}$$

The load torque in the shaft is calculated in (Foss et al., 1989) using experimental data. It can be represented as a function of the drag due to the engine friction (c_{de}), the aerodynamic drag (c_{dv}), and the selected gear ratio (gr) :

$$\begin{aligned} T_l &= (c_{de} + c_{dv} gr) N^2 \ , \\ c_{df} &= 0.00015, \ \text{drag due to the engine friction} \ (\tfrac{Nm \cdot sec^2}{rad^2}), \\ c_{dv} &= 0.001, \ \text{aerodynamic drag} \ (\tfrac{Nm \cdot sec^2}{rad^2}), \text{ and} \\ gr &= 0.197 \ \text{(3rd gear)}. \end{aligned} \tag{9}$$

The total inertia is a combination of the engine inertia (J_e), and the vehicle inertia reflected through the drivetrain, and is given by:

$$\begin{aligned} J &= J_e + m_v (r_w gr)^2 \ \tfrac{Nm \cdot sec^2}{rad} \ \text{where,} \\ J_e &: \text{engine inertia,} \\ m_v &: \text{vehicle mass} \\ r_w &: \text{wheel radius} \\ gr &: \text{gear ratio} \end{aligned} \tag{10}$$

On the basis of vehicle data, $J_e = 0.14 \ \frac{Nm\,sec^2}{rad}$, $m_v = 920 \ kg$, and $r_w = 0.28 \ m$ were estimated.

4 Nonlinear Breathing Process.

This section concentrates on the nonlinear dynamics of the engine breathing process. The study of the breathing process behavior is used to investigate and determine the operating regions where the secondary actuators (θ_c) have control authority in regulating the air charge into the cylinders. The air charge for every intake event is a function of the mass air flow rate into the cylinders and the engine speed, and it is directly related to the torque produced throughout the power stroke. Control over the transient and steady state values of the mass air flow is necessary to meet the objectives of good torque tracking and maintaining the A/F at stoichiometry. The signal θ_c must influence the static and dynamic behavior of the manifold pressure, the air flow into the manifold through the primary throttle position, and the air flow into the cylinders through the secondary actuators.

For the basic model (without the secondary actuators), the steady state operating point occurs at the intersection of the two trajectories of the mass air flow rates. This point is the nominal point shown in Fig. 3. The secondary actuators scale the engine pumping rate ($\dot{m}_{air}$) based on Eq. 4. Figure 3 shows the new trajectories of the air flow rate into the cylinders and the resulting new equilibria (set points in Fig. 3) for the breathing process. For sufficiently large $\theta_c < 1$, the steady state value of the mass air flow into the cylinder $\dot{m}_{cyl}$ is adjusted by causing the new equilibrium to shift from the sonic flow regime to the subsonic region. A closer investigation of the two regimes illustrates their significance in the new control scheme.

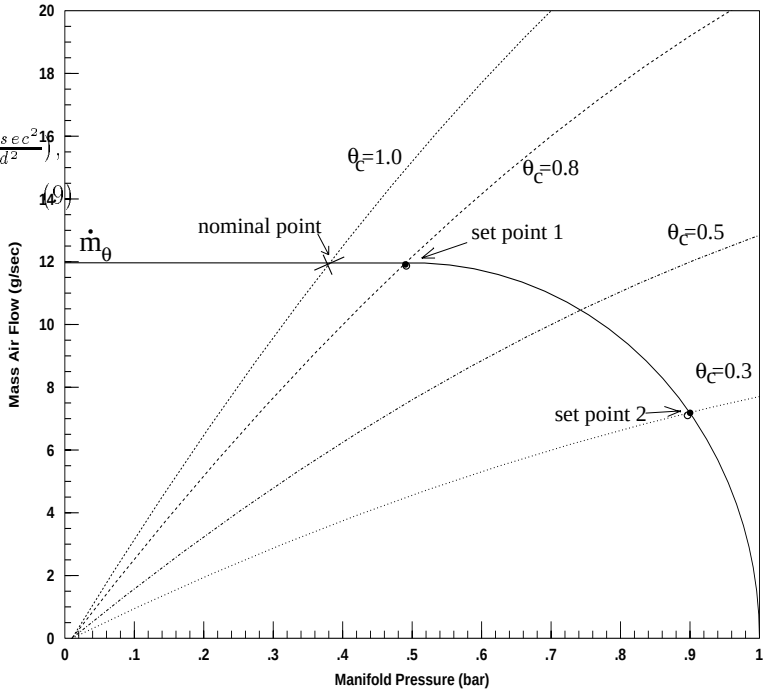

Figure 3: Trajectories of the air flow into the manifold ($\dot{m}_\theta$ for $\theta = 10$) and the air flow out of the manifold ($\dot{m}_{cyl}$) for several values of secondary actuators (θ_c). Engine speed is fixed $N = 300$ rad/sec.

When the flow through the primary throttle body is sonic and therefore does not depend on the manifold pressure, engine operation is in the flat region of $\dot{m}_\theta$ in Fig. 3. Small changes in θ_c cause no change in the steady state value of the mass air flow in and out of the manifold. For this reason, when the model of the breathing process is linearized, the secondary actuators have zero control authority on regulating the steady state mass air flow into the cylinders. This can be shown by the following transfer function between the control signal $\Delta\theta_c$ and the mass air flow into the cylinder $\Delta\dot{m}_{cyl}$ (see Fig. 4) :

$$\frac{\Delta\dot{m}_{cyl}(s)}{\Delta\theta_c(s)} = \frac{1}{1 + \frac{k_m k_1}{s}} = \frac{s}{s + k_m k_1}. \tag{11}$$

The DC gain of the above transfer function is clearly

zero. The usual technique of incorporating an integrator to regulate the steady state mass air flow into the cylinders cannot be used here, since the transfer function has a zero at the origin that cancels the integrator pole. It is also instructive to see this on a block diagram level. Figure 4 shows the linear dynamics of the breathing process for sonic flow after the introduction of the secondary actuators. Note that the integrator loop, which is an intrinsic part of the manifold dynamics in sonic flow, rejects the signal θ_c in steady state. Thus, the control signal $\Delta\theta_c$ cannot adjust the air charge into the cylinder by "smoothing" the effect of rapid throttle changes. Consequently, in sonic flow, the control command $\Delta\theta_c$ has zero control authority on the A/F and the steady state value of the engine torque.

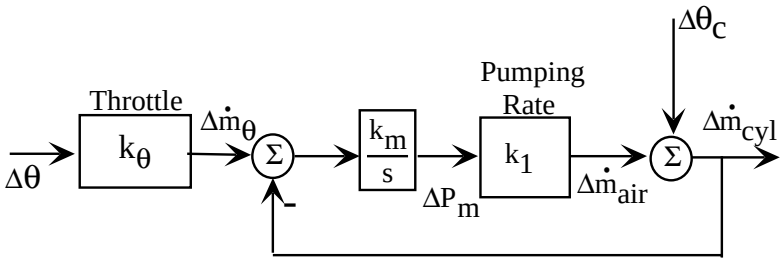

Figure 4: Block diagram of the linearized breathing process.

In the case where the flow is subsonic, i.e., $P_m/P_o > 0.5$, the air flow into the manifold depends on the primary throttle position and on the manifold pressure; thus, the linear model of the engine breathing process is different from the above, and the application of multivariable integral control is possible. The slope of the function that describes $\dot{m}_\theta$ (see Fig. 3) indicates the control authority of its operating point. It is clear now that the control authority of the secondary actuators around the set-point 2 in Fig. 3 is preferable to that around the set-point 1. Around set-point 2, the secondary actuators can be used to "smooth" the abrupt changes of air flow by regulating the air flow rate into the cylinders at a slower rate.

In conclusion, a nonlinear feedforward design of the θ_c set-points that allows operation in the subsonic flow regime, where the secondary actuators have maximal control authority, is necessary. This map will provide the steady state position of the new control variables.

5 Feedforward Control Design.

The natural nominal position of the secondary actuators is wide open, i.e., $\theta_c = 1$. However, recall from Section 4, that under these conditions the secondary actuators often have zero control authority in adjusting the steady state value of the mass air flow into the cylinders. A solution that uses a control signal (θ_c), which consists of a nonlinear feedforward term ($\theta_{c_{fw}}$) plus a feedback term ($\theta_{c_{fb}}$) is proposed. The feedforward design ensures that the secondary actuators have control authority over the steady-state value of cylinder flow over all possible engine conditions.

The nonlinear feedforward term ($\theta_{c_{fw}}$) is designed to satisfy the following three conditions: (i) it is a smooth and non-decreasing function of the primary throttle position (θ) and the engine speed (N), i.e., $\theta_{c_{fw}} = \theta_{c_{fw}}(\theta, N)$; (ii) the engine should deliver its maximum power output when operated at or close to wide open throttle (WOT), and (iii) maximal control authority should be available without sacrificing combustion stability and performance. To achieve these objectives over a wide range of engine operating conditions, one should consider the effects of combustion stability, thermodynamic performance indices and idle operating conditions. Also, as discussed previously, depending on the actuation scheme, the higher manifold pressure associated with the secondary actuators may result in higher volumetric efficiency. Presently such an extended analysis has not been completed. Based only on a control authority analysis, the following map has been developed for all engine speeds (see Fig. 5):

$$\theta_{c_{fw}} = \begin{cases} 0.55 \\ 0.6445 - 0.0126 \cdot \theta + 1.3125 \cdot 10^{-4} \cdot \theta^2 + 2.1875 \cdot 10^{-} \\ 1 - (\frac{\theta - 60}{65})^2 \\ 1 \end{cases}$$

The reasoning behind this map is briefly explained. First, usual driving conditions in urban areas correspond to partly open primary throttle (θ) interrupted by rapid requests for acceleration and deceleration (which are the main causes of A/F excursion). At partly open throttle, the maximum power of the engine is not required and hence $\theta_{c_{fw}} < 1$ is acceptable. In addition, $\theta_{c_{fw}}$ has been adjusted to ensure that the breathing process is operating near set-point 2 in Fig. 3. When the primary throttle is at or near WOT, the secondary actuators must smoothly operate close to the wide open position to ensure that maximum engine output can be achieved. Under WOT conditions, $P_m/P_o \approx 1$. Therefore, the secondary actuators are operating in the maximal control authority region, however, they have freedom of movement only towards one direction. The secondary actuators can reduce the steady-state cylinder air flow rate and reg-

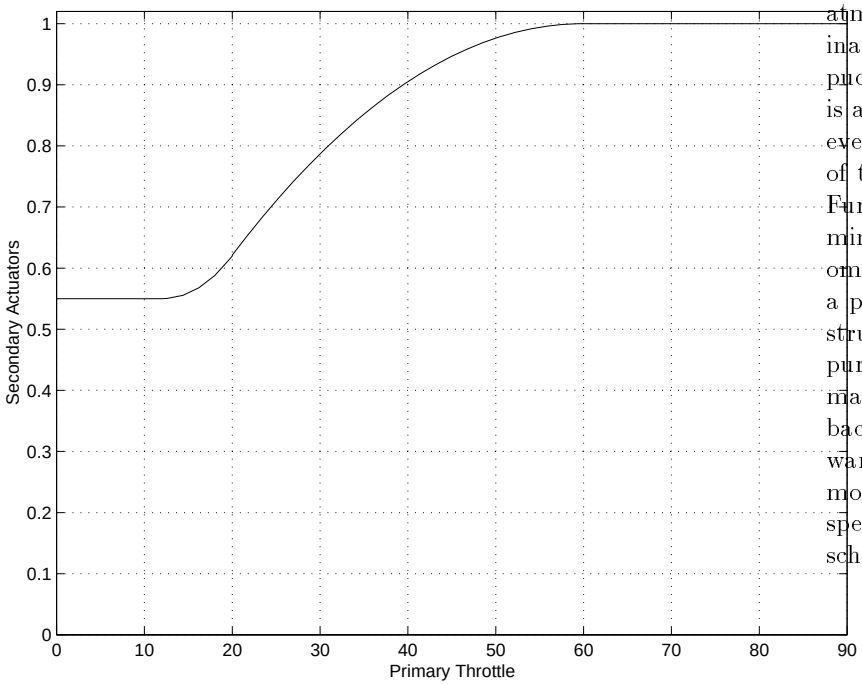

Figure 5: Static feedforward nonlinear term of the secondary actuators control signal (θ_c).

ulate the transient cylinder air flow rate during acceleration to cause lower A/F excursions. On the other hand, not much can be done when the driver closes the primary throttle: the secondary actuators cannot open further ($0 < \theta_c \leq 1$) to "smooth" the abrupt decrease of the air flow into the manifold by providing additional air. Finally, when the primary throttle is nearly closed, there is a minimum position for the secondary actuators below which combustion stability issues have to be addressed at different engine speeds. These issues will have to be addressed when a particular actuator has been selected, and, then, on a case-to-case basis.

The nonlinear feedforward scheme derived in this section clearly indicates the control authority problems that have to be surpassed in a system utilizing primary and secondary actuators to the engine flow. The contribution of the additional actuator to the overall vehicle performance needs further investigation. A thermodynamic evaluation is needed to determine the interaction of the new control variables with the various engine performance indices. An initial assessment of the influence of the suggested feedforward scheme shows that the feedforward term is beneficial to the manifold dynamics. The engine operates at $P_m/P_o \approx 0.9$, i.e., manifold almost fully charged, which causes considerably faster manifold filling dynamics during part throttle driving. This can be seen by evaluating the time constant of the breathing dynamics at several operating points (see Fig. 3). Achieving fast quasi-steady conditions close to atmospheric pressure in the intake manifold can eliminate wide variation in the time constant of the fuel puddling dynamics. A reduction of the pumping losses is also expected due to the low manifold vacuum, however the additional complication in the intake system of the engine might decrease the volumetric efficiency. Further investigation of all the above issues will determine the effect of the new control scheme on fuel economy. Our results on the A/F control of a system with a primary throttle and secondary actuators will be instrumental to such an experimental effort. For control purposes, usage of the feedforward term shown in Fig. 5 makes linearization fruitful and allows local linear feedback design. To elaborate on this point, the feedforward term ensures engine operation at low vacuum for most operating conditions, thus reducing the number of speed/load points that need to be included in the gain scheduling of the linear controllers.

6 Demand Map.

In the engine with the secondary actuators, the input is the primary throttle position (driver's command). It is measured but not controlled. The torque set-point (T_{des}) is calculated from the primary throttle position (θ) and the engine speed (N) measurements. This requires a demand map, similar to the one used in DBW schemes (Emtage et al., 1991), to determine the torque set-point for any throttle position and engine speed. This map is a nonlinear and well-defined map, i.e., torque has a unique value for specific throttle position and engine speed. For the purposes of this study, the demand map was generated by simulating the model of the conventional engine (without the secondary actuators) for different throttle positions and gear ratios, and recording the corresponding steady-state torque and engine speed response. The torque from the demand map will be used as the desired torque when the torque error is calculated to adjust the control signals.

7 Feedback Control Design.

This section serves as an assessment of the potential of the secondary cylinder air flow actuators in A/F control. To establish a reference for their potential ability to regulate A/F, we provide simple control designs of the same engine with currently used actuators. The A/F closed-loop response of the engine with the secondary actuators (θ_c-scheme) is compared to (i) the conventional[2] A/F closed-loop response (F_c-scheme),

[2] This scheme is called conventional because only the fuel command is used to control A/F to stoichiometry during rapid

and (ii) to the A/F closed-loop response of an engine equipped with electronic throttle (DBW-scheme). The comparison is based on simulation results using the nonlinear dynamic model described in Section 3. In this section, three linear multivariable controllers are designed for the three different schemes.

The main objective of the three control designs is to minimize A/F excursions during rapid changes in throttle pedal position, with zero steady state error. This is achieved with integral control, by augmenting the states of the system with the integral of A/F error. A secondary objective for the closed-loop performance of the engine with the secondary actuators, as well as the engine with the electronic throttle, is to maintain good torque response during transients. Good torque response amounts to (i) maintaining similarity of the rate of torque change in the first phase of the acceleration-deceleration with the conventional engine torque response, (ii) avoiding torque hesitation during the acceleration phase, and (iii) achieving the desired torque response in steady-state. This latter is accomplished with the introduction of the torque error in the control design of the engine with the secondary actuators (θ_c-scheme), and in the control design of the engine with the electronic throttle (DBW-scheme). Ensuring that the θ_c and DBW schemes have torque response similar to the conventional an important objective and cannot be ignored the two schemes can "decouple" the driver from the engine (in particular, from the cylinders). Without a torque objective, these control schemes would try to filter any rapid changes in air charge (lowpass the disturbance) to minimize A/F excursions causing very slow engine torque response. Thus, designing the two schemes based on A/F regulation only will cause unacceptable drivability.

The three schemes can be summarized as :

> **F_c-scheme :** During acceleration/deceleration, the driver changes the primary throttle position (θ), and fuel command is used to minimize A/F excursions caused by the rapid changes in the throttle position. The fuel regulation is based on A/F, torque, and throttle position measurements (multiple-input single-output controller, MISO controller). The A/F is measured using a linear EGO sensor.
>
> **θ_c-scheme :** As above, the driver controls the primary throttle position (θ), and the controller regulates secondary actuators (θ_c) and fuel command (F_c) to minimize A/F excursions and maintain good torque response. The control signal is calculated based on the nonlinear feedforward term and the linear feedback term ($\theta_c = \theta_{c_{fw}} + \theta_{c_{fb}}$). The same measurements are used as above, i.e., A/F, torque, and throttle position measurements.
>
> **DBW-scheme :** In this scheme, the driver controls the pedal position, and the controller regulates the throttle position (θ_e), and the fuel command (F_c) to precisely control A/F and track the torque demand (T_{des}). The measurements used in this scheme are identical to the ones used in the previous schemes.

The control structure of the three different schemes is schematically shown in Fig. 6.

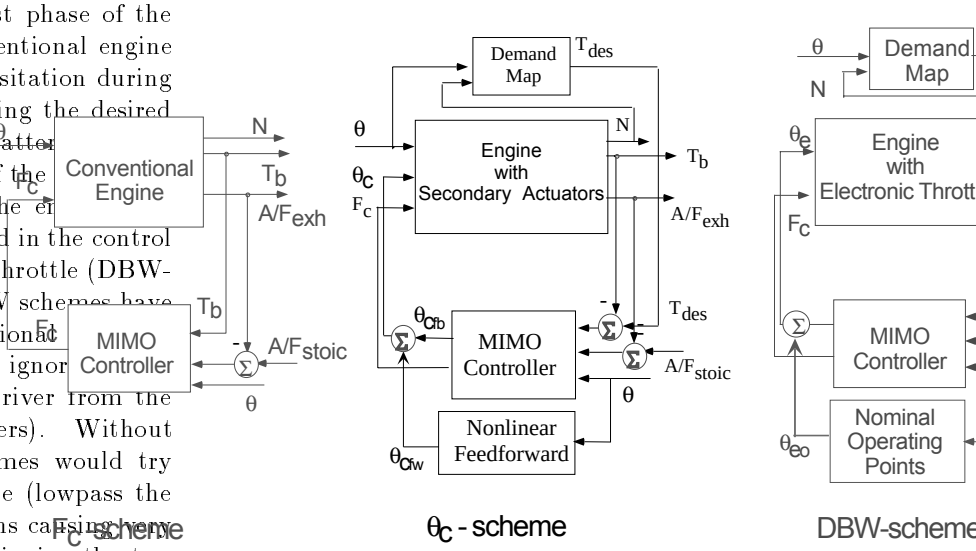

Figure 6: Schematic representation of the three control schemes.

In each case, we designed a linear multivariable feedback controller using LQG/LTR methodology. For the engine equipped with secondary actuators and the engine equipped with electronic throttle, we first augmented integrators to the A/F and torque outputs to guarantee zero steady state error. Appendices A and C describe the linear feedback controller for the engine with secondary actuators and the engine with electronic throttle respectively. For the engine with conventional A/F control, we only augmented an integrator to the A/F output. The feedback control design is given in Appendix B.

The engine model was linearized about an operating point that lies in the acceleration curve of the engine, and third gear was used in the powertrain rotational dynamics. The nominal primary throttle position used was $\theta = 20^o$, and the nominal set-point for the secondary actuators was 61% open, resulting in manifold

changes in throttle position. In the other two schemes ("non-conventional") fuel and air flow are jointly managed to maintain stoichiometry. Although the F_c-scheme is called "conventional" A/F control, neither the control strategy nor the measurements used are as in a conventional commercial vehicle.

pressure $P_m = 0.96$ bar. The air flow into the cylinders was 15.4 g/sec at 3000 RPM producing 31.5 Nm of torque. The same amount of torque is produced by the conventional engine at a primary throttle position of $\theta = 11.8^o$, with a manifold pressure of 0.51 bar. Note that the operating point that corresponds to $\theta = 11.8^o$ and $\theta_c = 100\%$ open (conventional operation) falls into the low control authority region explained in Section 4. For consistency in the comparisons, we designed all three controllers to achieve the best possible closed-loop response of A/F_{exh} to an output A/F disturbance. However, since the control loop structures (topologies) are so distinct, we cannot expect similar transient performance. For example, in the F_c-scheme the torque response cannot be modified significantly, whereas, in the DBW-scheme the torque response can be greatly modified and air-flow disturbances from the throttle to the A/F loop can be attenuated. Similarly to the DBW-scheme, the θ_c-scheme offers the potential advantages of having control authority over the air charge, and thus being able to coordinate both A/F and torque via independent air charge and fuel actuation. In the DBW-scheme, the throttle to torque ($\theta \rightarrow T_q$) response is specified based on the DBW-actuator time constant, which is considerably larger than the expected time constant of the secondary actuators used in the θ_c-scheme (we assume that the actuators that can realize secondary cylinder air flow control have to be crank-angle based mechanisms, hence very fast). Simulation results for the three control schemes are shown in the next section to illustrate their relative performance. A more in-depth discussion of the underlying mechanisms which determine the key features of their performance is also provided.

Robustness of the three control designs to actuator uncertainty is an important issue of the feasibility of the different control configurations. The engine model used in the design of the multivariable controller includes neither the θ_c actuator dynamics nor the electronic throttle actuator dynamics. Furthermore, there is a great level of uncertainty in the fuel puddling dynamics. At this preliminary stage, we do not have sufficient information to merit a comprehensive robustness analysis/synthesis procedure. The LQG/LTR methodology we use has been studied extensively for its robustness properties with respect to such uncertainty (Zhang and Freudenberg, 1990). For the purposes of this paper, we tested robustness simply by studying performance degradation with some additional dynamics inserted into the loop. Additional robustness studies would of course have to be performed as the model is developed further.

8 Simulation Example.

The purpose of this section is to illustrate some of the properties of the closed-loop system using the secondary actuators, and compare them with the conventional and drive by wire systems. Our purpose is to show that secondary actuators can yield potentially favorable response when compared to the other schemes. A complete study of the relative merit of the different engine configurations is beyond the scope of this paper.

Figure 7 is a simulation of the nominal response of the θ_c-scheme and the F_c-scheme for a 10% step change in primary throttle position, which corresponds to 16% step change in torque demand. The θ_c-scheme has $\pm 0.14\%$ A/F excursion and essentially zero A/F and torque error after 50 intake events. A dynamic model of the catalytic converter is needed to evaluate the effects of these A/F excursions to tailpipe emissions. The dynamic catalytic converter response depends on the amplitude and the frequency of the A/F excursions, and a control oriented model of this behavior was not available when this work was done. The integrated absolute error of A/F during a rapid throttle movement can be used, however, as a measurement of engine emissions during that period. The integrated error of A/F for the F_c-scheme is 0.0402 and for the θ_c-scheme is 0.0051 showing a 83% reduction in integrated A/F error. Also, the engine reaches the specified torque faster than in the F_c-scheme, improving drivability significantly. Note that the conventional fuel pulse width duration control cannot affect the torque performance of the engine.

It is important to note here that the θ_c-based MIMO controller allows simultaneous improvement of both T_q and A/F response, even-though it is well known that there is an inherent tradeoff between fast torque response and small A/F ratio. It is also true that the secondary actuators cannot eliminate this tradeoff because the addition of actuators cannot change the limitation due to the long delay in the fuel feedback loop. It is known that multivariable controllers can achieve different tradeoffs between interacting loops. This is explained in the context of a related automotive application in (Stefanopoulou et al., 1995; Stefanopoulou et al., 1999). In particular, the θ_c MIMO controller uses the additional degree of freedom that the cross-coupling mechanisms provide to better cancel the disturbance from the air loop to the fuel loop.

The simulation in Fig. 8 shows the closed loop torque and A/F performance for the θ_c-scheme and the DBW-scheme. Both responses are well within the high-efficiency window of the catalyst, though the absence of the lean spike in the A/F in tip-in conditions in the DBW-scheme is immediately noticeable. In DBW throttle systems, the engine is decoupled from the disturbances caused by the rapid throttle movements

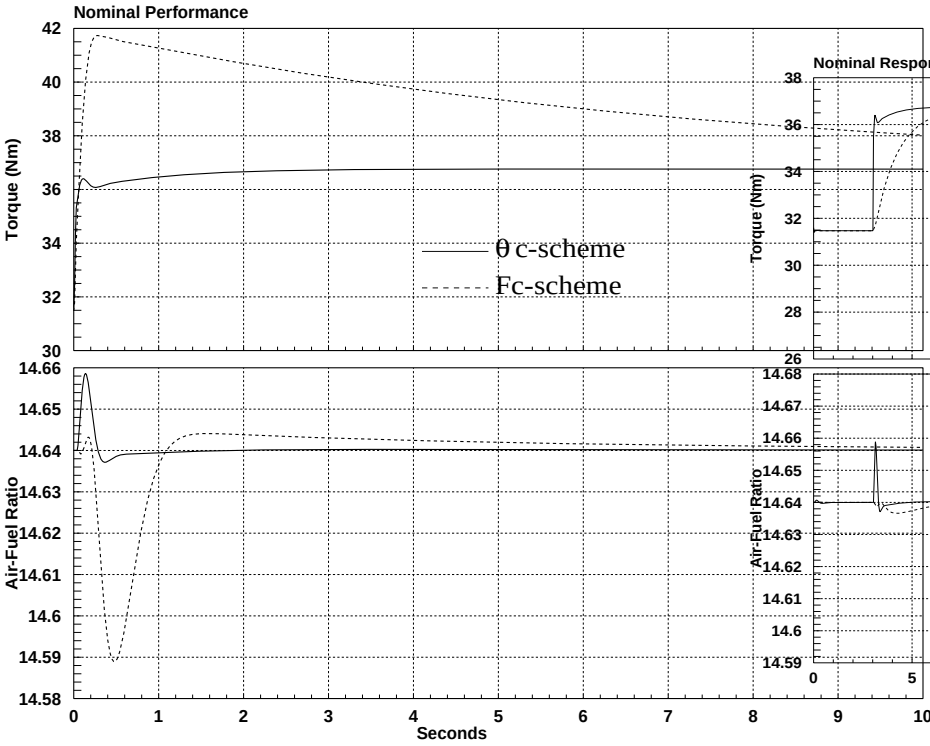

Figure 7: Simulation of the θ_c-scheme and F_c-scheme.

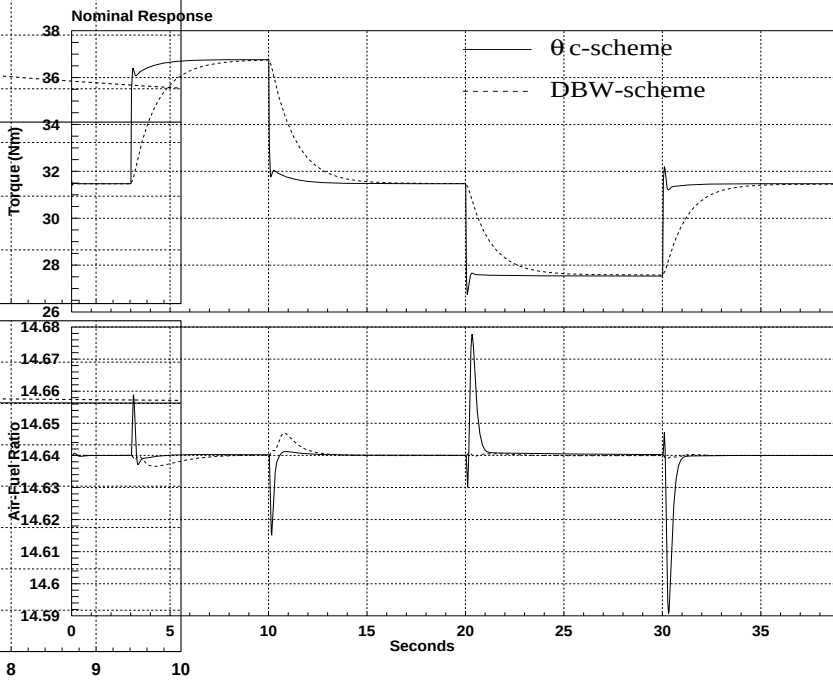

Figure 8: Closed loop response of the θ_c-scheme and DBW-scheme for a square wave in the demanded torque.

which are imposed by the driver due to the slow DBW-actuator. This isolated the high bandwidth torque demands resulting in smooth A/F control. To maintain the same good A/F results with secondary actuators would require a smoother (slower) torque response in the engine which can be achieved by detuning the air loop. The correct tradeoff between A/F and drivability can be defined only after a rigorous study of the emissions for an FTP cycle and the driver's feel. We include here the simulations in Fig. 8 as a point of reference in a future comprehensive comparison.

The performance of the θ_c-scheme was also tested under uncertainty in the fuel puddling dynamics due to its importance in accurate transient A/F control. Figure 9 shows the torque and A/F response of the above control schemes using a time constant of 0.2 sec in the puddling dynamics (see Section 3 for the nominal value). The simulation results show a limited performance degradation of the closed loops, however the θ_c-scheme maintains the improvement of the torque response better than the other two methods. The same comparative results between the F_c-scheme and the θ_c-scheme are present: integrated A/F error in F_c-scheme is 0.0547, and in θ_c-scheme is 0.0084. The A/F response of the DBW-scheme slightly degrades and the A/F integrated error is 0.0085. Therefore, the θ_c-scheme maintains emissions results comparable to the DBW-scheme.

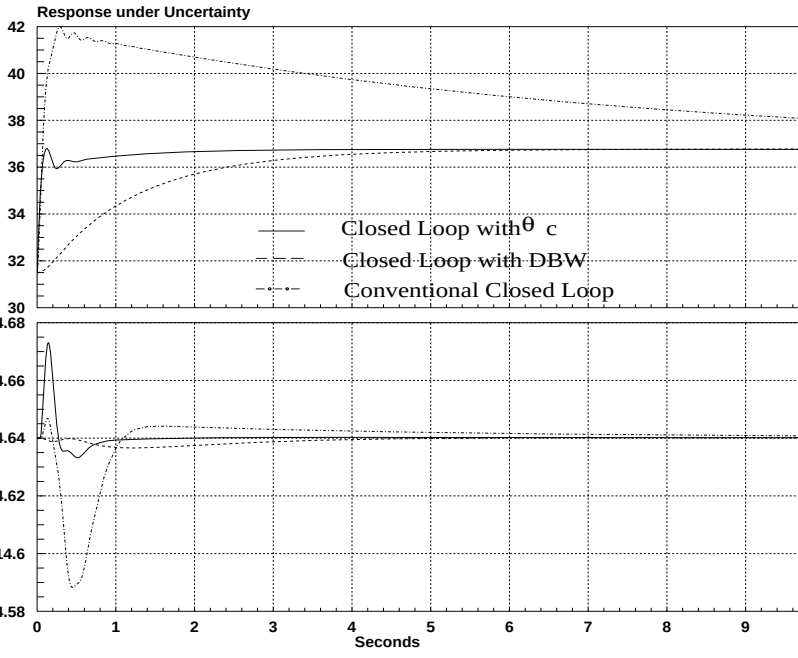

Figure 9: Closed loop performance under uncertainty in the fuel puddling dynamics.

9 Conclusions.

In this paper, an existing nonlinear dynamical engine model was modified to include the effects on performance of secondary actuators placed before the intake ports of the cylinders. It was shown that different operating regions yield different levels of control authority for regulating the steady-state air flow into the cylinders. This result, although well known in the thermodynamic community, has not been acknowledged by control engineers. It represents an important consideration in designing cylinder air flow control schemes when the primary throttle is regulated by the driver (throttled operation).
The analysis carried out here emphasized global (nonlinear) issues in the design of the feedforward portion of the controller, in order to improve actuator authority for the ensuing feedback design, and to exploit the physics of the manifold filling dynamics for potential fuel economy gains. The feedback design then focused on a single operating point, in order to determine the potential dynamic benefits of the joint management of air and fuel at (or near) the intake valve level; it was shown to promise enhanced drivability and air-to-fuel ratio control. The secondary actuators may thus provide an alternative solution to electronic throttles. A global analysis of the feedback design problem is a subject of ongoing research.

References

Aquino C. F., 1981, "Transient A/F Control Characteristics of the 5 Liter Central Injection Engine," SAE Paper No. 810494.

Ashhab M. S., Stefanopoulou A. G., Cook J. A., and Levin M., "Camless Engine Control for Robust Unthrottled Operation," SAE Paper No. 981031.

Bidan P., Boverie S., and Chaumerliac V., "Nonlinear Control of a Spark Ignition Engine," IEEE Trans. Control Systems Technology, Vol. 3, No. 1, pp. 4-13.

Chang C.-F., Fakete N. P., and Powell J. D., "Engine Air-Fuel Ratio Control Using an Event-Based Observer," SAE Paper No. 930766.

Crossley P. R. and Cook J. A., "A Nonlinear Model for Drivetrain System Development," IEE Conference 'Control 91', Edinburgh, U.K., March 25-28, 1991. IEE Conference Publication 332 Vol. 2, pp. 921-925.

Emtage A. L., Lawson P. A., Passmore M. A., Lucas G. G. and Adcock P. L., "The Development of an Automotive Drive-By-Wire Throttle System as a Research Tool," SAE Paper No. 910081.

Foss A. M., Heath R. P. G., Heyworth P., Cook J. A. and McLean J., "Thermodynamic Simulation of a Turbocharged Spark Ignition Engine for Electronic Control Development," Proc. of the Inst. Mech. Eng. Seventh International Conference on Automotive Electronics, London, U.K., C391/044, pp. 195-202.

Gray C., "A Review of Variable Engine Valve Timing," SAE Paper No. 880386.

Grizzle J. W., Cook J. A. and Milam W. P., "Improved Transient Air-Fuel Ratio Control using Air Charge Estimator," Proc. 1994 Amer. Contr. Conf., Vol. 2, pp. 1568-1572.

Hendricks E., Jensen M., Kaidatzis P., Rasmussen P., and Vesterholm T., "Transient A/F Ratio Error in Conventional SI Engines Controllers," SAE Paper No. 930856.

J. B. Heywood, *Internal Combustion Engine Fundamentals,* McGraw-Hill, 1988.

Kang J. and Grizzle J. W., "Engine Air-fuel-ratio and Torque Control by using Secondary Throttles," *Advances in Automotive Control,* Proc. of IFAC Workshop, pp. 203-210.

J. Kang and J. W. Grizzle, "Nonlinear Control of Joint Air and Fuel Management in a SI Engine," submitted to 1999 American Control Conference.

Ma T. H., "Effects of Variable Engine Valve Timing on Fuel Economy," SAE Paper No. 880390.

Manz P.-W., "Influence of a Rapid Throttle Opening on the Transient Behavior of an Otto Engine," SAE Paper No. 922234.

Moraal P. E., "Adaptive Compensation of Fuel Dynamics in an SI Engine using a Switching EGO Sensor," Proc. 1995 Conf. on Decision and Control, pp. 661-667, New Orleans.

Moraal P. E., Cook J. A., and Grizzle J. W., "Modeling the induction process of an automobile engine," *Control problems in industry,* Lasiecka I. and Morton B., Ed., Birkhauser, pp. 253-270, 1995.

Moraal P. E., Grizzle J. W. and Cook J. A., "An Observer for Single-Sensor Individual Cylinder Pressure Control," Proc 1993 Conf. on Decision and Control, Vol. 3, pp. 2955-2961.

Nishiyama R., Okhubo S. and Washino S., "An Analysis of Controlled Factors Improving Transient A/F Ratio Control Characteristics," SAE Paper No. 890761.

Novak J. M., "Simulation of the Breathing Process and Air-Fuel Ratio Distribution Characteristics of Three-Valve, Stratified Charge Engines," SAE Paper No. 770881.

Powell B. K. and Cook J. A., "Nonlinear Low Frequency Phenomenological Engine Modeling and Analysis," Proc. 1987 Amer. Contr. Conf., Vol 1, pp. 332-340.

Powell J. D., "Engine Control Using Cylinder Pressure: Past, Present and Future," Journal of Dynamic Systems, Measurements and Control, Vol. 115, pp. 343-350.

Prabhakar R., Citron S. J. and Goodson R. E., "Optimization of Automobile Engine Fuel Economy and Emissions," ASME Paper 75-WA/Aut-19.

Prabakhar R., "Optimal and Suboptimal Control of Automotive Engine Efficiency and Emissions," Ph.D. Thesis 1975, Purdue University, West Lafayette, IN.

Schecter M. M. and Levin M. B., "Camless Engine," SAE Paper No. 960581.

K. Srinivasan, G. Rizzoni, M. Trigui and G.-C. Luh, "On Line Estimation of net Engine Torque from Crankshaft Angular Velocity Measurements Using Repetitive Estimators," Proc. 1992 Amer. Contr. Conf., Vol. 1 ,pp. 516-520.

Stefanopoulou A. G., Butts K. R., Cook J. A., Freudenberg J. S., and Grizzle J. W., "Automotive Powertrain Control for Modular Controller Architectures : A Case Study," Proc. 1995 Conference on Decision and Control, pp. 768-773.

Stefanopoulou A. G., Freudenberg J. S., and Grizzle J. W., "Variable Camshaft Timing Engine Control," to appear in the IEEE Transactions on Control System Technology.

Turin R. and Geering H. P., "Model-based Adaptive Fuel Control in an SI Engine," SAE Paper 940374.

Tuttl J. H., "Controlling Engine Load by Means of Late Intake-Valve Closing," SAE Paper No. 800794.

Vogel O., Roussopoulos K., Guzzella L., and Czekai J., "An Initial Study of Variable Valve Timing Implemented with a Secondary Valve in the Intake Runner," SAE Paper No. 960590.

Zhang Z. and Freudenberg J. S., "Loop Transfer Recovery for Nonminimum Phase Plants," IEEE Trans. on Automatic Control, Vol. 35, No. 5, pp. 547-553.

Appendix

A Feedback Control Design using Secondary Actuators

The engine model with the secondary actuators is linearized at throttle position equal to 20 degrees, secondary actuators equal to 61% open, engine speed equal at 3000 rpm. The state variables of the linearized model are manifold pressure, A/F at the EGO sensor, mass air flow, angular velocity, fuel puddle, and states associated with second order Padé approximation of the delays in the processes and signals. The state space representation of the linearized model of the engine with the secondary actuators is given by :

$$\begin{aligned} \dot{x}(t) &= Ax(t) + Bu(t) + B_r r(t) \\ y(t) &= Cx(t) \end{aligned} \tag{12}$$

where $u = \begin{bmatrix} \theta_c \text{ (sec. actuators)} \\ F_c \text{ (fuel command)} \end{bmatrix}$, $r = \theta$ (primary throttle)

and $y = \begin{bmatrix} T_b & \text{(torque meas.)} \\ A/F_{exh} & \text{(meas. at the EGO sensor)} \end{bmatrix}$,

where, matrices A, B, B_r, and C are given below:

$$A = \begin{bmatrix} -0.079 & 139.786 & 0 & 0 & 0 & -1.013 & 0 \\ 0.019 & -100 & 10.7952 & 0 & 0 & 0 & 0 \\ -0.0289 & 0 & -74.61 & 0 & 0 & 0 & 0 \\ 0 & 0 & 0 & -6.667 & 0 & 2 & 0 \\ -0.0001 & 0 & -0.485 & 0 & -7.692 & 0 & 0 \\ 0 & 0 & 0.01 & 0 & -1.587 & -0.001 & 0 \\ 0 & 0 & 0 & 0 & 0 & 0 & 61.40 \\ 0 & 0 & 0 & 0 & 0 & 0 & -0.0333 \\ 0 & 0 & 0 & 333.33 & 0 & 0 & 0 \\ 0. & 0. & 0. & 0. & 0. & 0. & 0. \\ 0 & 0 & 0 & 0 & 3.846 & 0 & 0 \end{bmatrix}$$

$$B' = \begin{bmatrix} 0 & 25.9675 & -10.2811 & 0 & 0 & 2.361e+03 & 0 & 0 & 0 & 0 & 0 \\ 0 & 0 & 0 & 0 & 0 & -8.254e+04 & 0 & 0 & 0 & 0 & 2 \end{bmatrix}$$

$$B'_r = \begin{bmatrix} 0 & 0.4908 & 0.3622 & 0 & 0.0038 & 44.6284 & 0 & 0 & 0 & 0 \end{bmatrix},$$

$$C = \begin{bmatrix} -0.0231 & 410.86 & 0 & 0 & 0 & -2.978 & 0 & 0 & 0 & 0 & 0 \\ 0 & 0 & 0 & 0 & 0 & 0 & 0 & 0 & 0 & 2.5 & 0 \end{bmatrix}.$$

During changes in throttle position, it is important to maintain A/F at stoichiometry and maintain zero tracking error in the torque response. This is accomplished by augmenting the state vector with the integral of the error in the A/F response ($\dot{q}_2 = A/F_{exh} - A/F_{stoic}$), and the integral of the error in the torque response ($\dot{q}_1 = T_{b_m} - T_{b_{des}}$). The input and state vector are augmented as follows: $\hat{r}' =$

$\begin{bmatrix}\theta & T_{b_{des}} & A/F_{stoic}\end{bmatrix}$, and $\hat{x}' = \begin{bmatrix}x' & q'\end{bmatrix}$. The resulting augmented system is :

$$\underbrace{\begin{bmatrix}\dot{x}\\ \dot{q}\end{bmatrix}}_{\dot{\hat{x}}} = \underbrace{\begin{bmatrix}A & 0\\ C & 0\end{bmatrix}}_{\hat{A}}\underbrace{\begin{bmatrix}x\\ q\end{bmatrix}}_{\hat{x}} + \underbrace{\begin{bmatrix}B\\ 0\end{bmatrix}}_{\hat{B}}u + \underbrace{\begin{bmatrix}B_r & 0\\ 0 & -I\end{bmatrix}}_{\hat{B}_r}\hat{r}, \quad (13)$$

The controller feedback gains in $u = -K\hat{x} = \begin{bmatrix}-K_1 & -K_2\end{bmatrix}\begin{bmatrix}x\\ q\end{bmatrix}$ is found by solving the LQR problem:

$$K_1 = \begin{bmatrix}0.0004 & 0.0411 & 0.0060 & 0.0156 & -0.0173 & 0.0000 & 0.0000 & 0.0000 & 0.0004 & 0.0190 & -0.0352\\ 0.0000 & 0.0023 & -0.0122 & -0.0247 & 1.8198 & -0.0004 & -0.0001 & -0.0001 & 0.0014 & -0.0816 & 2.1547\end{bmatrix}$$

$$K_2 = \begin{bmatrix}0.0099 & 0.0450\\ 0.0014 & -0.3130\end{bmatrix}$$

For the complete LQG/LTR controller design, one needs to estimate the states (x) using a Kalman filter. The real symmetric positive semi-definite matrix representing the intensities of the state noises Q_{xx}, and the real symmetric positive definite matrix representing the intensities of the measurement noises Q_{yy} were assumed diagonal. Loop transfer recovery in the input was employed and the resulting observer gain is given below:

$$L' = \begin{bmatrix}0.2582 & 0.0001 & -0.0001 & -0.4108 & 0.0016 & -6.3386 & -56.4934 & 6.4796 & -0.5916 & -0.0322 & 0.0018\\ -0.6951 & -0.0001 & 0.0003 & 0.3324 & 0.0000 & 0.2615 & 79.6739 & -0.3080 & 0.0001 & -0.0001 & -0.5737\end{bmatrix}$$

B Fuel Feedback Control Design

The control structure of the conventional fuel control configuration is shown in Section 6. The engine model described in Section 3 without the secondary actuators was used. The model is linearized at throttle position equal to 11.8 degrees, and engine speed equal to 3000 rpm. The state space representation of the linearized model is given by:

$$\begin{aligned}\dot{x}(t) &= Ax(t) + Bu(t) + B_r r(t)\\ y(t) &= cx(t)\end{aligned} \quad (14)$$

where $u =$ F_c (fuel command), $r = \theta$ (primary throttle), and
$y =$ A/F_{exh} (meas. at the EGO sensor).

The matrices A, B, B_r, and C used in the open loop system are given below:

$$A = \begin{bmatrix}-0.079 & 139.785 & 0 & 0 & 0 & -1.013 & 0\\ 0.0173 & -100 & 26.852 & 0 & 0 & 0 & 0\\ -0.0280 & 0 & -10.908 & 0 & 0 & 0 & 0\\ 0 & 0 & 0 & -6.67 & 0 & 2 & 0\\ -0.0001 & 0 & -0.0019 & 0 & -7.692 & 0 & 0\\ 0 & 0 & 0.024 & 0 & -1.5874 & -0.001 & 0\\ 0. & 0. & 0. & 0. & 0. & 0. & 100\\ 0 & 0 & 0 & -222.2 & 0 & 0 & -33.\\ 0. & 0. & 0. & 0. & 0. & 0. & 0.\\ 0 & 0 & 0 & 0 & 3.84 & 0 & 0\end{bmatrix}$$

$$B' = \begin{bmatrix}0 & 0 & 0 & 0 & 0 & -8254.3 & 0 & 0 & 0 & 2\end{bmatrix},$$

$$B_r' = \begin{bmatrix}0.0000 & 0.0000 & 0.8710 & 0.0000 & 0.0060 & 0.0000 & 0.0000 & 0\end{bmatrix}$$

$$c = \begin{bmatrix}0 & 0 & 0 & 0 & 0 & 0 & 0 & 0 & 2.5000 & 0\end{bmatrix}.$$

The control objective in the conventional engine (A/F control is based on regulating the fuel flow) is to maintain A/F at stoichiometry during changes in pedal position. For this reason, we used integral control, and the augmented the input and state vector are given by : $\hat{r}' = \begin{bmatrix}\theta & A/F_{stoic}\end{bmatrix}$, and $\hat{x}' = \begin{bmatrix}x' & q\end{bmatrix}$. The resulting augmented system is :

$$\underbrace{\begin{bmatrix}\dot{x}\\ \dot{q}\end{bmatrix}}_{\dot{\hat{x}}} = \underbrace{\begin{bmatrix}A & 0\\ c & 0\end{bmatrix}}_{\hat{A}}\underbrace{\begin{bmatrix}x\\ q\end{bmatrix}}_{\hat{x}} + \underbrace{\begin{bmatrix}B\\ 0\end{bmatrix}}_{\hat{B}}u + \underbrace{\begin{bmatrix}B_r & 0\\ 0 & -1\end{bmatrix}}_{\hat{B}_r}\hat{r}, \quad (15)$$

The gains of the designed LQR controller are given below:

$$K_1 = \begin{bmatrix}0 & 0 & -0.027 & -0.035 & 1.877 & -0.0006 & 0.0016 & 0.0045 & -0$$

$k_2 = -0.949$, and the gain of the designed observer is:

$$L' = \begin{bmatrix}-18.2527 & 1.2789 & 0.4568 & -0.0001 & 0.0059 & -20.1610 & 4.7\\ -0.8831 & 0.0004 & 0.0022 & 0.3602 & 0.0000 & 0.0494 & -12$$

C Feedback Control Design using Electronic Throttle.

In an engine equipped with a electronic throttle, the driver controls the accelerator pedal position, but the actual throttle position that regulates the air flow into the manifold is electronically controlled. The engine model described in Section 3 is modified to include the new control command, and linearized at throttle position equal to 11.8 degrees, engine speed equal at 3000 rpm. The state space representation of the linearized model is given by :

$$\begin{aligned}\dot{x}(t) &= Ax(t) + Bu(t)\\ y(t) &= Cx(t)\end{aligned} \quad (16)$$

$$\text{where } u = \begin{bmatrix}\theta_e \text{ (electr. thr. command)}\\ F_c \text{ (fuel command)}\end{bmatrix}, \text{ and} \quad (17)$$

$$y = \begin{bmatrix}T_b & \text{(torque measurement)}\\ A/F_{exh} & \text{(meas. at the EGO sensor)}\end{bmatrix}. \quad (18)$$

The matrices A, B, B_r, and C are given below:

$$A = \begin{bmatrix} -100 & 26.852 & 0 & 0 & 0 & 0 & 0 & 0 & 0.017 & 0 \\ 0 & -10.908 & 0 & 0 & 0 & 0 & 0 & 0 & -0.028 & 0 \\ 0 & 0 & -6.667 & 0 & 2 & 0 & 0 & 0 & 0 & 0 \\ 0 & -0.002 & 0 & -7.692 & 0 & 0 & 0 & 0 & -0.0001 & 0 \\ 0 & 244.19 & 0 & -1.587e+05 & 0 & 0 & 0 & 1.575 & 0 & 0 \\ 0 & 0 & 0 & 0 & 0 & 100 & 900 & 0 & 0 & 0 \\ 0 & 0 & -222.22 & 0 & 0 & -33.33 & -233.33 & 0 & 0 & 0 \\ 0. & 0. & 0. & 0. & 0. & 0. & 2. & -5. & 0. & 0. \\ 139.786 & 0 & 0 & 0 & -1.013 & 0 & 0 & 0 & -0.076 & 0 \\ 0 & 0 & 0 & 3.846 & 0 & 0 & 0 & 0 & 0 & -10 \end{bmatrix},$$

$$B' = \begin{bmatrix} 0.0000 & 0.8710 & 0.0000 & 0.0060 & 0.0000 & 0. & 0. & 0. & 0. & \\ 0.0000 & 0.0000 & 0.0000 & 0.0000 & -82543 & 0. & 0. & 0. & 0. & 2. \end{bmatrix},$$

$$C = \begin{bmatrix} 410.86 & 0 & 0 & 0 & -2.978 & 0 & 0 & 0 & 0.023 & 0 \\ 0 & 0 & 0 & 0 & 0 & 0 & 0 & 2.5 & 0 & 0 \end{bmatrix}.$$

Changes in the accelerator pedal position imposed by the driver represent changes in the demanded torque. For an electronically throttled engine, the driver is disconnected from the engine, and does not cause "disturbances" in the A/F loop. However, good engine torque response must be maintained to satisfy drivability requirements. Zero steady state torque error is accomplished by augmenting the states with the integral of the error in the torque response. In this control scheme, A/F control is limited only by sensor/actuator limitations and uncertainties in the modeling. The control design followed is similar to the earlier design in Appendix A. The controller feedback gains and the observer gain L are given below:

$$K_1 = \begin{bmatrix} 0.4046 & 0.9368 & 0.1478 & -0.0005 & 0.00 & -0.0016 & -0.0047 & 0.1574 & -0.0233 & -0.0009 \\ 2.7691 & -0.8089 & -0.5292 & 1.9192 & -0.0290 & 0.0199 & 0.0551 & -2.277 & -0.0005 & 3.0441 \end{bmatrix}$$

$$K_2 = \begin{bmatrix} 0.1000 & 0.3135 \\ 0.0031 & -9.9951 \end{bmatrix}, \text{ and}$$

$$L' = \begin{bmatrix} 0.0000 & -0.0001 & -0.4094 & 0.0016 & -6.3390 & 7.3912 & -0.5880 & -0.0300 & 0.2397 & 0.0018 \\ 0.0004 & 0.0020 & 0.3463 & 0.0000 & 0.3095 & -11.4118 & 1.3235 & 0.4716 & -0.8408 & -0.0001 \end{bmatrix}.$$